Renewable Energy and Power Quality Journal
https://repqj.com/index.php/repqj/index
RE&PQJ, Vol. 23, No. 2, 2025

# Smooth Gradient Control of Signal Ripple at the Output Side of a Charging Pile Based on Small-signal Scattering Characteristics

Zheng Chang[1], Chao Zhang[2,*], Peng Tao[2], Yangrui Zhang[2], Xiaoyu Liu[2], Shasha Zhao[2]

[1]State Grid Hebei Electric Power Co., Ltd., Shijiazhuang, 050000, China
[2]State Grid Hebei Marketing Service Center, Shijiazhuang, 050000, China
[*]Corresponding author's email: zhangcheng45120938@163.com

**Abstract.** The signal ripple on the output side of a charging pile is prone to large fluctuations due to load changes, leading to unstable current, abnormal battery charging, and reduced battery lifespan. The small-signal scattering characteristics can reflect the charging pile's response to load fluctuations, and controlling these characteristics can help mitigate signal ripple fluctuations. To achieve this, a smooth gradient control method for the output-side signal ripple of the charging pile is proposed, based on small-signal scattering characteristics. First, the main circuit model of the Superbuck converter of the charging pile is constructed, and the small-signal model is generated by selecting the input and state variables from the model. The small-signal scattering characteristic of the converter is analyzed in the input small-signal perturbation by using the model, and the relationship between the characteristic and the signal ripple component of the output side is obtained. Based on the analysis, the amplitude gain of the transferring derivative is selected as the control parameter. Then, the PID controller parameters are optimized using the gradient descent method to minimize the output-side signal ripple. The results show that this method effectively controls the ripple component of the current signal on the output side of the charging pile under low-frequency perturbation at different output voltages. By adjusting the transfer derivative amplitude gain, the output-side signal ripple is significantly smoothed. The average reduction of the ripple component after the smoothing can be up to 0.275 A, ensuring stable output from the charging pile.

**Key words.** Small signal, Scattering characteristics, Charging pile, Output side signal, Transfer conductance, PID controller

## 1. Introduction

As an important infrastructure for electric vehicles, the performance and safety of charging piles have received increasing attention [1]. On the output side of the charging pile, the ripple phenomenon is particularly significant because the charging pile needs to convert the AC power supply to the DC power supply and charge the battery of the electric vehicle [2,3]. In this process, owing to the influence of many factors such as power conversion, filter circuit design, and load change, the output-side signal generates a certain ripple [4]. The ripple of the output signal of the charging pile will lead to the instability of voltage or current, which not only affects the accuracy and safety of the charging process and leads to the undercharging or overcharging of the battery, but also increases the heat generation of the battery and shortens the service life of the battery [5]. Therefore, studying control methods for output-side signal ripple is crucial for improving charging quality, extending battery life, and ensuring charging pile stability and reliability [6].

Current research in this field primarily focuses on signal modulation techniques for AC-AC converters. Jeelani et al. [7] constructed a main circuit model of an AC-AC converter and combined it with space vector modulation (SVM) to control the switching tubes' operation. By adjusting the duty cycle of the switching tubes, they achieved stable output voltage modulation. However, the high-frequency switching action may generate electromagnetic interference, resulting in an adjustment error in the duty cycle, leading to a modulation deviation of the final output voltage signal. Sangmin et al. studied the voltage signal balance control method for series resonant converter [8]. They constructed the basic circuit of a series resonant converter and adjusted the output voltage duty cycle and operating frequency using pulse-width modulation (PWM) and pulse-frequency modulation (PFM). This approach regulated the phase-shift angle and frequency while utilizing sensors to collect output voltage or current signals for feedback control. Sensors were used to collect the output voltage or current signals and feed back to the PWM and PFM modulators, which were adjusted to complete the balanced control of the voltage signals.The PFM changed the output voltage by adjusting the pulse frequency. When the output voltage fluctuated due to the load change, the PFM could not realize the precise

control of the voltage signals of the converter. The closed-loop control method of the inductive buck converter proposed by Siripan et al. [9] created the basic circuit of the inductive buck converter, which was most suitable for an inductive buck converter. The basic circuit structure of inductive buck converter was created, the PWM closed-loop controller was used to adjust the switching duty cycle, the output voltage was collected as the feedback signal, the error signal was calculated, and the PWM closed-loop controller was adjusted by the error signal to complete the closed-loop control of inductive buck converter. Mehrdad et al. [10] introduced a closed-loop control method for the DC-side conductance of multilevel converters. They developed a property model for the multilevel converter, analyzed the relationship between DC-side conductance and voltage, and selected a PI controller based on the analysis results to implement closed-loop control. The performance of the PI controller depended mainly on its parameter settings, which were usually set under specific load conditions. When the load changed, the PI controller exhibits poor adaptability to the load change and could not maintain stability or achieve the desired control effect. Al et al. proposed an FPGA control method for fractional-order systems and PID controllers [11]. By using fractional-order systems and control, the concept of fractional calculus had been implemented in modeling and control design, and applied to practical applications. However, converting these memory-dependent systems and controllers into hardware presented challenges, so they were typically used only for higher-order integer systems.

The small-signal scattering characteristics reflect the dynamic response characteristics of the charging pile converter to the perturbation of small signals at different frequencies [12]. Analyzing the relationship between these characteristics and the signal ripple component on the output side of the charging pile can provide an effective basis for accurate and robust control of the signal ripple on the output side of the charging pile [13]. The PID controller, or Proportional-Integral-Derivative (PID) controller, is an important control algorithm in the field of industrial control, primarily composed of proportional, integral, and derivative units [14]. Its main advantages include a simple structure, ease of implementation, wide application, and independence from control parameters, making it widely used in various industrial control fields [15]. In this study, the application of the PID controller in charging station systems holds significant importance. By adopting a PID controller that can quickly respond to error changes, its proportional unit can eliminate steady-state errors, the integral unit can predict the trend of error changes, and the derivative unit can accurately regulate the output signal of the charging station, effectively suppressing signal fluctuations. Additionally, gradient descent is an optimization algorithm based on function gradient information, commonly used in machine learning and artificial intelligence for recursive approximation of the least deviation model [16,17]. Its advantages include simple computation and easy implementation.

Based on this, a smooth gradient control of the output signal ripple of the charging pile based on the small signal scattering characteristics is proposed. The specific contributions of the proposed method are described as follows:

Firstly, a complete main circuit model of the charging station and Superbuck inverter is proposed, and the state Equation is derived through Kirchhoff's law, followed by the construction of a small signal model. The relationship between the small signal scattering characteristics and output ripple of the inverter is quantified by selecting inductor current and capacitor voltage as state variables and duty cycle as control variables.

Secondly, based on the small signal model, the transfer conductance amplitude gain characteristics of the Superbuck inverter are analyzed, revealing its direct impact mechanism on the output side ripple.

Thirdly, a PID controller based on gradient descent method is designed, with the transmission of conductance amplitude gain as the control parameter. Ripple suppression is achieved by dynamically optimizing the proportional, integral, and differential coefficients, ensuring the safety and stability of the charging process. This provides a new approach for signal control at the output end of charging stations, further promoting the development of charging infrastructure.

At the same time, this paper summarizes the abbreviations in the text and gives the corresponding full English names. Please refer to Table 1 for details.

Table 1. Abbreviations

| Abbreviation | Full Name |
|---|---|
| PID | Proportional-Integral-Derivative |
| SAE | Society of Automotive Engineers |
| DC | Direct Current |

## 2. Charging Pile Output Side Signal Ripple Smoothing Gradient Control

### *A. Modeling of Charging Pile and Superbuck Converter Structure*

The charging pile structure mainly contains a Superbuck converter, three-phase uncontrolled rectifier circuit, PID controller, feed-forward controller, and other parts [18]. Its structure is shown in Figure 1.

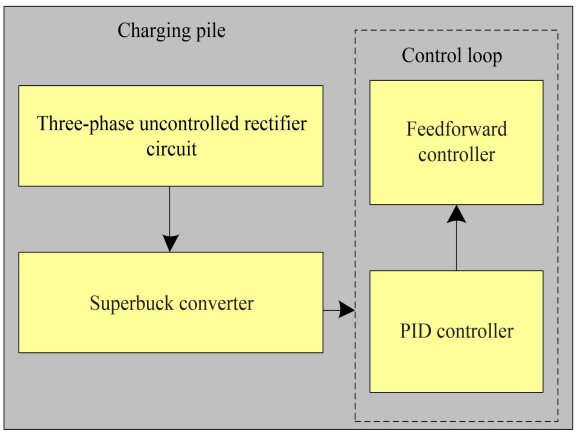


Figure 1. Charging pile structure diagram.

Among them, the Superbuck converter, as the backstage converter of the charging pile and represents the key module in the charging pile. Its output response characteristics, that is, its small-signal scattering characteristics in response to small-signal perturbation of the input can directly affect the stability of the signal ripple on the output side of the charging pile [19]. Therefore, to achieve smooth gradient control of the signal ripple at the output side of the charging pile, it is necessary to analyze the small-signal scattering characteristics of the buck converter and use it as a control variable to realize [20]. The main circuit topology of the buck converter in the charging pile is illustrated in Figure 2.

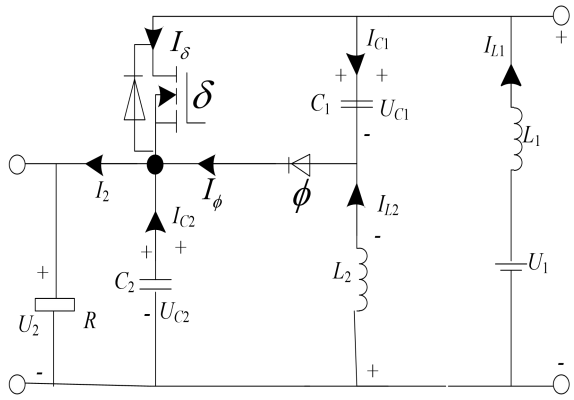


Figure 2. Topological structure diagram of main circuit of Superbuck converter of charging pile.

In the figure, $C$ and $L$ denote the capacitance and inductance of the buck converter in the charging pile, respectively; $U_1$ and $U_2$ denote the input and output voltages, respectively; $\delta$ and $\phi$ denote the switching tube and the continuity diode, respectively; $R$ indicates resistance; $I_2$ indicates the output current; $I_L$ and $I_C$ denote the input inductance and capacitance current, respectively; $I_\delta$ and $I_\phi$ denote the currents of the switching tube and continuity diode, respectively; $U_C$ indicates the capacitive voltage. When the switching tube $\delta$ in the Superbuck converter is turned on, its dual inductors charge, while the first capacitor $C_1$ discharges. During this time, its renewing diode $\phi$ turns off. Conversely, when its switching tube $\delta$ turns off, the energy of the first inductor $L_1$ passes through the capacitor $C_1$, making the continuous flow diode $\phi$ turn off and turn on. The formula for the duty ratio $x$ is

$$x = U_2 / U_1 \quad (1)$$

Combining Kirchhoff's voltage and current laws can lead to the Equation corresponding to Figure 2 as:

$$\begin{cases} U_1 - L_1 \mathrm{d}I_{L_1}/\mathrm{d}t = U_{C_1} + L_2 \mathrm{d}I_{L_2}/\mathrm{d}t, I_{L_1} = C_1 \mathrm{d}U_{C_1}/\mathrm{d}t + I_\delta \\ I_\phi = C_1 \mathrm{d}U_{C_1}/\mathrm{d}t + I_{L_1}, U_2/R = I_\phi + C_2 \mathrm{d}U_{C_2}/\mathrm{d}t + I_\delta \end{cases} \quad (2)$$

Organizing Equation (2) can be given:

$$\begin{cases} \mathrm{d}I_{L_1}/\mathrm{d}t = \left[U_1 - U_{C_2} - U_{C_1} + U_{C_1}\lambda\right]/L_1, \mathrm{d}I_{L_2}/\mathrm{d}t = \left(U_{C_1}\lambda - U_{C_2}\right)/L_2 \\ \mathrm{d}U_{C_1}/\mathrm{d}t = \left[I_{L_1} - I_{L_1}\lambda - I_{L_2}\lambda\right]/C_1, \mathrm{d}U_2/\mathrm{d}t = \left(I_{L_1} + I_{L_2} - U_{C_2}/R\right)/C_2 \end{cases} \quad (3)$$

Where $\lambda$ denotes the coupling coefficients of each variable in the main circuit of the Superbuck converter. For ease of description, the state variables of the Superbuck converter are represented by vector groups as:

$$\boldsymbol{Z} = \left[I_{L_1}, I_{L_2}, U_{C_1}, U_{C_2}\right] \quad (4)$$

### *B. Small-signal Scattering Characterization of Superbuck Converter for Charging Pile Based on Small-Signal Model*

The impedance, frequency, and stability of the converter to the perturbed small signal are characterized by the small-signal scattering characteristics of the charging pile Superbuck converter [21-23] when the charging pile buck converter is operated in the steady-state interval and its input or output is perturbed by a small signal. These small-signal scattering characteristics are typically characterized by a transfer function, where the transfer conductance serves as the primary transfer function. The amplitude gain of this transfer conductance effectively represents the small-signal scattering behavior of the charging pile's Superbuck converter in response to perturbations. Using the Superbuck converter model developed in the previous section as an example, we select the inductance current $I_L$ and the capacitor voltage $U_C$ as state variables, the input voltage $U_1$ as the input variable, and the duty cycle $x$ as the control variable to construct the small-signal model [24,25] of the charging pile's Superbuck converter. This model is used to analyze the transfer conductor amplitude gain of the Superbuck converter to cope with the small-signal perturbation, and the small-signal scattering characteristics of the converter are obtained. Based on

the obtained results, we investigate how the transfer conductance amplitude gain affects the output-side signal ripple components. The transfer conductance amplitude gain is subsequently adopted as a control parameter for output-side signal ripple regulation. A PID controller is then designed to manipulate the Superbuck converter's transfer conductance amplitude gain, thereby achieving desired small-signal scattering characteristics for the charging pile.

With the selected variables above, the state-space equation for the charging pile's Superbuck converter small-signal model, constructed using the state-space averaging method, is:

$$\begin{bmatrix} s\tilde{I}_{L_1}(s) \\ s\tilde{I}_{L_2}(s) \\ s\tilde{U}_{C_1}(s) \\ s\tilde{U}_{C_2}(s) \end{bmatrix} = \begin{bmatrix} 0 & 0 & (x-1)/L_1 & 1/L_1 \\ 0 & 0 & (x)/L_2 & -1/L_2 \\ (1-x)/C_1 & -x/C_1 & 0 & 0 \\ 1/C_2 & 1/C_2 & 0 & -1/RC_2 \end{bmatrix} \begin{bmatrix} \tilde{I}_{L_1}(s) \\ \tilde{I}_{L_2}(s) \\ \tilde{U}_{C_1}(s) \\ \tilde{U}_{C_2}(s) \end{bmatrix} + \begin{bmatrix} 1/L_1 & U_{C_1}/L_1 \\ 0 & U_{C_1}/L_2 \\ 0 & -I_2/C_1 \\ 0 & 0 \end{bmatrix} \begin{bmatrix} \tilde{U}_1(s) \\ \tilde{x}(s) \end{bmatrix} \tag{5}$$

In the formula, *s* denotes the small-signal scattering parameter of the Superbuck converter of the charging pile. Let the total inductor current be $\tilde{I}_L(s) = \tilde{I}_{L_1}(s) + \tilde{I}_{L_2}(s)$ . From Equation (5), the open-loop transfer function relating the output current to the input voltage in the charging pile's Superbuck converter can be derived as:

$$\tilde{I}_2(s)/\tilde{U}_1(s) = \tilde{U}_2(s)/R\tilde{U}_1(s) = \tilde{I}_L(s)/(RC_2s+1)\,\tilde{U}_1(s) = X_{I_LU}(s)/(RC_2s+1) \tag{6}$$

Where $X_{I_LU}(s)$ represents the transfer function from the input voltage to the total inductor current in the charging pile's Superbuck converter, i.e., the open-loop transfer conductance. This parameter characterizes the small-signal scattering behavior of the converter. As can be seen from Equation (6), the impact of the input voltage of the charging pile Superbuck converter on the output current and voltage can be reflected in the impact of the total inductor current. Therefore, the low-frequency ripple component of the output-side signal of the charging pile can be reduced by controlling the pulsation of the total inductor current caused by the disturbance of the input voltage of the charging pile Superbuck converter. The operator equation for the open-loop transfer conductor $X_{I_LU}(s)$ is

$$X_{I_LU}(s) = \tilde{I}_L(s)/\tilde{U}_1(s)\big|_{\tilde{x}(s)=0} = \frac{(L_2C_1C_2s^3)/U_1 + (L_2C_1s^2)/RU_1 + (C_2xs)/U_1 + x/RU_1}{\left[(L_1L_2C_1C_2s^4)/U_1 + (L_1L_2C_1s^3)/RU_1 + (C_2L_2(1-x)^2 + C_2x^2L_1)s^2/U_1 + (C_1L_1 + C_1L_2)s^2/U_1\right] + (L_2(1-x)^2 + x^2L_1)S/RU_1 + 1/U_1} \tag{7}$$

The closed-loop transfer conductance of this charging pile Superbuck converter is:

$$X_{I_LU1}(s) = \tilde{I}_L(s)/\tilde{U}_1(s)\big|_{\tilde{I}_{L_\varsigma}(s)=0} = X_{I_LU}(s)/(\alpha_I(s)+1) \tag{8}$$

In the formula, $I_{L_\varsigma}(s)$ denotes the current inner loop reference value of the charging pile; $\alpha_I(s)$ denotes the open-loop transfer function of the charging pile current loop; and $\alpha_I(s) = \beta_I(s)\beta_{IL_x}(s)\varphi_{\mathrm{PWM}}\gamma_I$ , of which, $\varphi_{\mathrm{PWM}}$ denotes the PWM modulator gain. Where $\gamma_I$ denotes the sampling factor of the output current; $\beta_I(s)$ denotes the transfer function of the PID controller within the charging pile; $\beta_{IL_x}(s)$ represents the transfer function of the total inductor current to the duty cycle. $\beta_{IL_x}(s)$ is expressed as follows:

$$\beta_{IL_x}(s) = \tilde{I}_L(s)/\tilde{x}(s)\big|_{\tilde{U}_1(s)=0} = \frac{[(RCs+1)/R]\{1 + (I_LL_2(1-x)s - I_LL_1xs)/U_1 + (C_1L_1s^2 + C_1L_2s^2)\}}{\left[(L_1L_2C_1C_2s^4)/U_1 + (L_1L_2C_1s^3)/RU_1 + (C_2L_2(1-x)^2 + C_2x^2L_1)s^2/U_1 + (C_1L_1 + C_1L_2)s^2/U_1\right] + (L_2(1-x)^2 + x^2L_1)S/RU_1 + 1/U_1} \tag{9}$$

Based on this, the transfer conductance of the charging pile Superbuck converter in response to small-signal perturbation representing the small-signal scattering characteristics is derived. According to Equation (8), the smaller the transfer conductance amplitude gain of the charging pile Superbuck converter under a small signal disturbance. The better the small-signal scattering characteristics of the converter are, and the smaller the fluctuation of the charging pile total inductor current caused by the input voltage disturbance. Therefore, by lowering the transfer conductor amplitude gain of the buck converter, the signal ripple component on the output side of the charging pile caused by input voltage perturbation can be effectively suppressed, and the signal ripple on the output side of the charging pile can be smoothly controlled.

### *C. Smooth Gradient Control of Signal Ripple at the Output Side of Charging Pile Based on Small Signal Scattering Characteristics of Superbuck Converter*

As in the above section, the PID controller is designed to reduce the amplitude gain of the transfer conductor of the Superbuck converter of the charging pile in response to input perturbations. This is done in order to prevent the ripple component of the signal on the charging pile's output side during the perturbation and to achieve smooth control of the ripple of the signal on the charging

pile's output side. The control parameter is the transfer guide amplitude $X_{I_LU}(s)$ gain, which can reflect the small signal scattering characteristics of the charging pile Superbuck converter. The structure of the charging pile PID controller designed in this manner is illustrated in Figure 3.

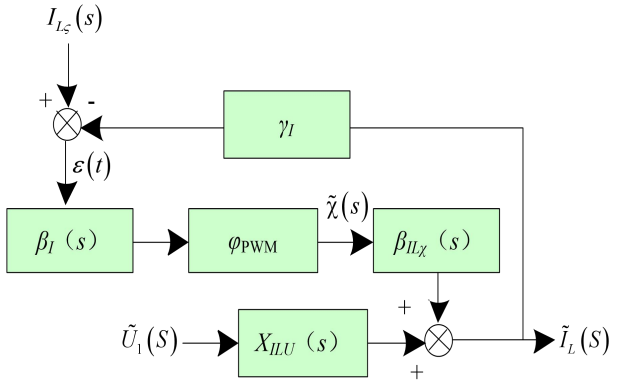


Figure 3. Charging pile PID controller structure diagram.

The control object of the charging pile PID controller is the transfer guide $X_{I_LU1}(s)$ amplitude gain of the charging pile Superbuck converter, which realizes comprehensive control of the charging pile Superbuck converter transfer conductor by constituting the control quantities of the differential, integral, and proportion of the deviation of the transfer conductor magnitude gain generated in the control process in a linear relationship. The equation for the control quantity $\omega(t)$ in the control process is

$$\omega(t)=k_p\varepsilon(t)+k_d\mathrm{d}\varepsilon(t)/\mathrm{d}t+k_i\int_0^t\varepsilon(t)\mathrm{d}t \quad (10)$$

Where $\varepsilon(t)$ denotes the transfer conductance amplitude gain deviation generated during the control process of the PID controller; $k_i$ , $k_p$ ,and $k_d$ indicate the integral, proportional, and differential coefficients of the charging PID controller, respectively.

The expression for the transfer function $\beta_I(s)$ of the charging pile PID controller is:

$$\beta_I(s)=\left(k_i/s\right)+k_p+k_d \quad (11)$$

Through the PID controller on the charging pile, the Superbuck converter transfers the conductor amplitude gain parameter adjustment and effectively inhibits the charging pile total inductor current fluctuation caused by small signal disturbance to realize the charging pile output side signal ripple effective smoothing control. To ensure optimal tuning of the PID controller's three key parameters (proportional, integral, and differential) and achieve superior control performance, we employ the gradient descent method for parameter optimization. This yields a gradient-optimized PID controller capable of smooth ripple control on the charging pile's output side. The optimization process mainly consists of two stages: the correction stage and the output stage, in which the correction stage mainly uses the gradient descent method to update and optimize the three key parameters of the PID controller, namely, the differential, integral, and proportional. The output stage maintains the fixed values of the parameters after updating and optimizing, and calculates the output of the criterion function SAE.

In the process of optimizing and adjusting the parameters of the PID controller using the gradient descent method, the solution of partial derivatives is the key problem, and the most important aspect of the gradient descent method is the distribution of the parameters in the entire PID controller. For the three key parameters of the PID controller, the partial derivatives of each parameter account for a different proportion, and the interaction between the partial derivatives of the parameters affects the calibration results of the gradient descent method. This can be realized by weighting the influence of each parameter on the entire PID controller. First, the criterion function SAE is considered as the performance index of the PID controller, and its operational equation is as follows:

$$\mathrm{SAE}=\sum_0^k g(k)-h(k) \quad (12)$$

In the formula, $g(k)$ and $h(k)$ denote the given PID controller input and output parameters, respectively.

Set $\mu$ denotes the learning step of the gradient descent method, and the correction of the PID controller parameters by the gradient descent method is:

$$\Delta k=-\mu\partial\mathrm{SAE}/\partial k \quad (13)$$

Therefore, the parameter modification equation of the PID controller for the gradient descent method is given by:

$$\begin{cases}\Delta k_p=-\mu\partial\mathrm{SAE}/\partial k_p\\ \Delta k_i=-\mu\partial\mathrm{SAE}/\partial k_i\\ \Delta k_d=-\mu\partial\mathrm{SAE}/\partial k_d\end{cases} \quad (14)$$

An approximation of Equation (14) yields:

$$\begin{cases}\partial\mathrm{SAE}/\partial k_p=\Delta\mathrm{SAE}/\Delta k_p=\left(\mathrm{SAE}_n-\mathrm{SAE}_{n-1}\right)/\Delta k_p\\ \partial\mathrm{SAE}/\partial k_i=\Delta\mathrm{SAE}/\Delta k_i=\left(\mathrm{SAE}_n-\mathrm{SAE}_{n-1}\right)/\Delta k_i\\ \partial\mathrm{SAE}/\partial k_d=\Delta\mathrm{SAE}/\Delta k_d=\left(\mathrm{SAE}_n-\mathrm{SAE}_{n-1}\right)/\Delta k_d\end{cases} \quad (15)$$

Where $SAE_n$ represents the PID controller performance index after the $n$ parameter optimization iteration of the gradient descent method; $SAE_{n-1}$ represents the performance index of the PID controller after the $n-1$ parameter optimization iteration of the gradient descent method.

Owing to the different weighting of the bias in the control process of the PID controller, the deviation $\Delta SAE/\Delta k_p$ of the proportionality parameter $k_p$ and the deviation $\Delta SAE/\Delta k_d$ of the differential parameter $k_d$ can be allocated according to the following formula:

$$\begin{cases} \Delta SAE/\Delta k_p = \left[\Delta k_p / \left(\Delta k_p + \Delta k_d\right)\right]\left(\Delta SAE/\Delta k_p\right) \\ \Delta SAE/\Delta k_p = \left[\Delta k_d / \left(\Delta k_p + \Delta k_d\right)\right]\left(\Delta SAE/\Delta k_d\right) \end{cases} \quad (16)$$

Similarly, the optimization of the three key parameters of the PID controller can be realized, and the values of the PID controller parameters after the optimization are:

$$\begin{cases} k_p(t+1) = k_p(t) + \Delta k_p \\ k_d(t+1) = k_d(t) + \Delta k_d \\ k_i(t+1) = k_i(t) + \Delta k_i \end{cases} \quad (17)$$

The optimized tuning process of the PID controller parameters based on the gradient descent method is illustrated in Figure 4.

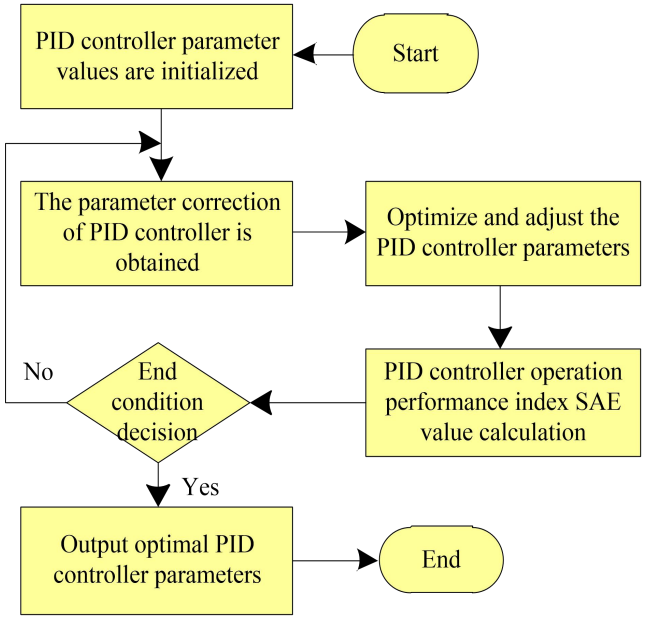


Figure 4. PID controller parameter optimization tuning process diagram based on gradient descent method.

The optimized tuning process of the PID controller parameters based on the gradient descent method is as follows:

(1) Initialization: the initial values of the three key parameters of the integral $k_i$, proportion $k_p$ and differential $k_d$ of the PID controller are $k_{i0}$, $k_{p0}$ and $k_{d0}$; the performance index SAE value for this PID controller operation is $SAE_2$; the previous time its operational performance index value is $SAE_1$.

(2) Calculate the performance index SAE value of the PID controller operation, the cumulative sum of the performance index value of each moment of each operation of the PID controller is as a performance index, and the performance index value in the gradient descent method of the parameter optimization and adjustment process is gradually reduced.

(3) PID controller parameter value updates, gradient descent method of PID controller parameter optimizes, and adjustment process is only at the beginning of each cycle. First, the PID controller proportional parameter $k_p$ increases the correction step by one, at which point the correction is $\Delta k_p$. According to Eqs. (14)–(17), the PID controller parameters are optimized, and the optimized proportional parameters $k_p$ are obtained. In this case, if the PID controller operates with a lower value of the performance index SAE, the proportional parameter $k_p$ continues to optimize; otherwise, the scale parameter $k_p$ changes in the opposite direction.

(4) In the same way to optimize and adjust the three parameters of the PID controller, two convergence error values $\psi$ and $\upsilon$ are set to check whether to reach the end conditions of parameter optimization. When the correction $\Delta k$ is less than a predetermined convergence error value $\psi$ and the difference between the SAE value (sum of errors) of the performance index of this PID controller runs and the last error is lower than the convergence error value $\upsilon$, then no further optimization of the integrating PID controller parameters is continued and the optimal PID controller parameters are obtained. The optimization of the integrating PID controller parameter values is continued until the end conditions are satisfied.

## 3. Analysis of Experimental Results

In order to verify the practical application effect of this method, a DC charging pile in an underground parking lot is selected as the experimental object. The output side signal ripple is smoothed and gradient controlled by this method. The key parameters of the charging pile are shown in Table 2.

Table 2. Details of key parameters of experimental charging pile.

| Parameter name | Parameter value |
|---|---|
| Input line voltage | AC 220V/50Hz |
| Maximum output voltage | 500V |
| Maximum output current | 10A |
| Overall efficiency | ≥90% |
| Maximum output power of the power supply system | 5000W |
| Maximum output current of the bridge | 18.9A |
| Rectifier output voltage | 311V |
| Input filter inductance | 2.5mH |
| Energy storage inductance | 4mH |
| PWM gain | 1/2.4 |
| Energy storage capacitance | 0.47μF |
| Output filter capacitance | 100μF |
| Rectifier bridge model | KBU3510 |
| Circuit type | Full bridge circuit |
| High-frequency transformer material | PO50/50 core of PC40 material |
| Number of turns in primary winding of high frequency transformer | 10-turn |
| Number of turns of secondary winding of high frequency transformer | 20-turn |
| Isolating capacitance | 2.2uF CBB capacitor |
| PWM converter type | Zero voltage PWM Converter (ZVS) |
| Full bridge inverter output maximum voltage | 500V |
| Full bridge inverter circuit output maximum current | 10A |

The calculation formula of the number of turns of the primary winding of high frequency transformer 10 in Table 2 is as follows:

$$N = \frac{V \times 10^8}{4.44 \times f \times B_m \times A_e} \quad (18)$$

In the formula, $V$ indicates the primary input voltage; $f$ indicates the working frequency; $B_m$ indicates the maximum magnetic flux density of the core; $A_e$ indicates the effective cross-sectional area of the core.

In addition, to avoid the impact of current and voltage delays, low-parasitic-inductance and low-capacitance effect power devices are selected in the hardware circuit design, thereby reducing the distributed parameters of the circuit that cause signal transmission delays. Furthermore, a feedforward control strategy is introduced at the control algorithm level. By predicting the trends of voltage and current changes in advance, control signals can be pre-adjusted to compensate for potential delays. Moreover, high-speed sampling and real-time feedback mechanisms are employed to ensure that the control system can quickly obtain accurate voltage and current information and respond swiftly.

The field experiment scenario for the smooth gradient control of the signal ripple on the output side of the experimental charging pile is shown in Figure 5.

Figure 5. Experimental scene diagram.

The experiment stipulates that the input line voltage of the charging pile is 220V (±10%) (50 Hz). When the input line voltage of the experimental charging pile is 220V, the spectral analysis results of the output voltage of the three-phase uncontrolled rectifier circuit are as shown in Figure 6.

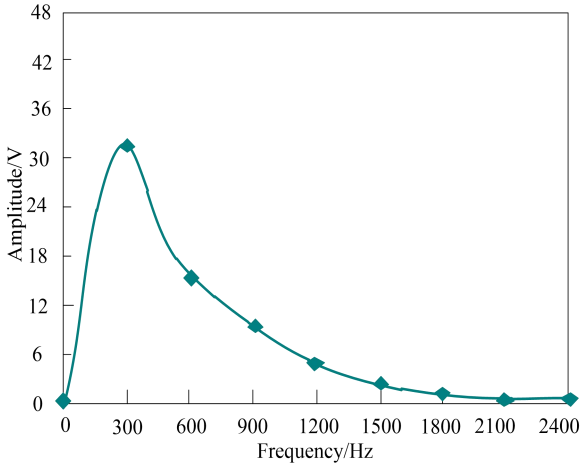


Figure 6. Spectrum analysis diagram of output voltage of three-phase uncontrolled rectifier circuit of experimental charging pile.

As can be seen in Figure 6, the output voltage of the three-phase uncontrolled rectifier circuit of the experimental charging pile contains 300 Hz and its 2x and 3x frequency harmonic components, that is, the main harmonic components are 300 Hz, 600 Hz, and 900 Hz, and the existence of such low-frequency harmonic components makes the signal on the output side of the Superbuck converter of the experimental charging pile charging interface have the corresponding frequency of unsmooth ripple components, seriously affecting the cycle service life of the loaded power battery pack.

The Bode plot of the Superbuck converter transfer conductance of the experimental charging pile under low-frequency harmonic component perturbations displayed in Figure 6 is shown in Figure 7.

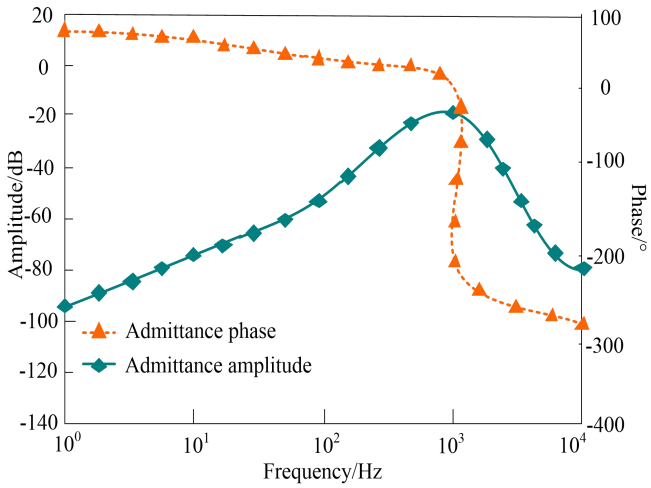


Figure 7. Transfer admittance Baud diagram of experimental charging pile converter.

Figure 7 shows that in the presence of low-frequency harmonic component perturbation. When the experimental charging pile is in the low-frequency band, the amplitude of the transfer conductor of the converter shows a rapid increase in the trend of the transfer conductor. The transfer conductor of the phase value of the transfer conductor shows a slow decline in the trend of the scattering characteristics of the experimental charging pile converter for the transfer conductor of the transfer conductor increases rapidly in the low-frequency band in the presence of harmonic component perturbation and the current from the voltage lag to exceed the voltage. The current is transformed to exceed the voltage.

The input line voltage of the experimental charging pile is 220V, and the output voltages of the converter are 300V and 500V respectively. The input voltage, output voltage, and output current signal waveforms of the charging pile converter are shown in Figure 8.

Figure 8 shows that when the input voltage of the experimental charging pile is fixed, the output voltage of the experimental charging pile converter is 300V and 500V with low-frequency harmonic component perturbation, the ripple of its output current signal is obviously unstable, and the highest ripple fluctuation of the output current signal under two kinds of output voltages is 0.37A and 0.55A, respectively.

Based on the preceding analysis, the proposed method successfully achieves smooth gradient control of output-side signal ripple in the experimental charging pile under disturbance conditions. The study specifically examines output current ripple components in the converter when operating at 300V and 500V output voltages, demonstrating the controller's effectiveness across different operating points. In the control process of this paper's method, it is necessary to first implement the gradient optimization to the parameters $k_p$ , $k_i$ and $k_d$ of the PID controller of this paper. The optimization process is shown in Figure 9.

Through the optimization process in Figure 9, the parameters $k_p$ , $k_i$ and $k_d$ of the PID controller for the control process of the method in this study are 0.1, 3000, and 0.23, respectively. The experimental charging pile converter transfer conductance as well as the output current signal waveforms after the control of the method in this study are shown in Figure 10.

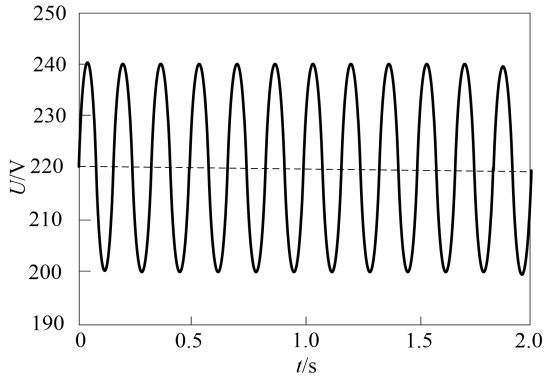


(a) Input voltage signal waveformof the charging pile converter

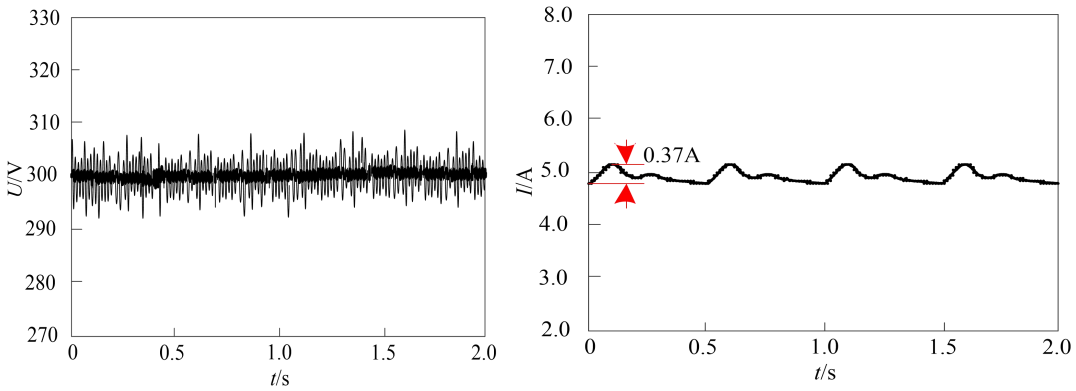


(b) When the output voltage is 300V, the output voltage and current signal waveforms of the charging pile converter.

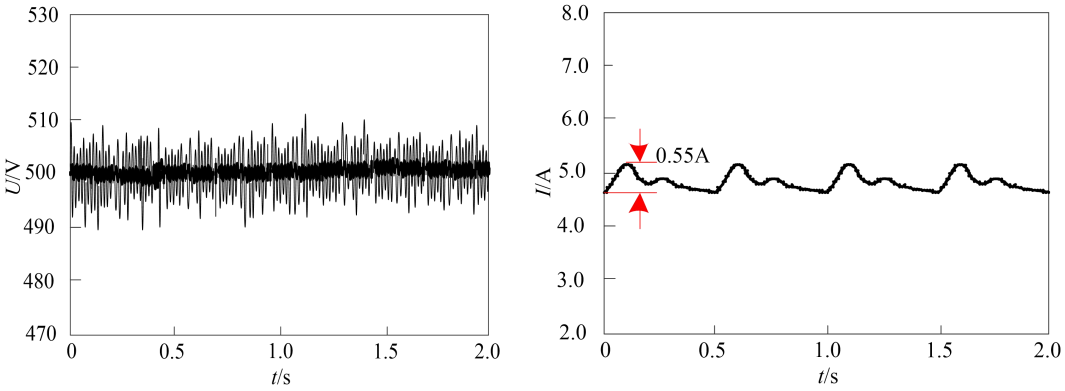


(c) When the output voltage is 500V, the output voltage and current signal waveforms of the charging pile converter.

Figure 8. Waveform diagram of input voltage, output voltage and output current signal of experimental charging pile converter.

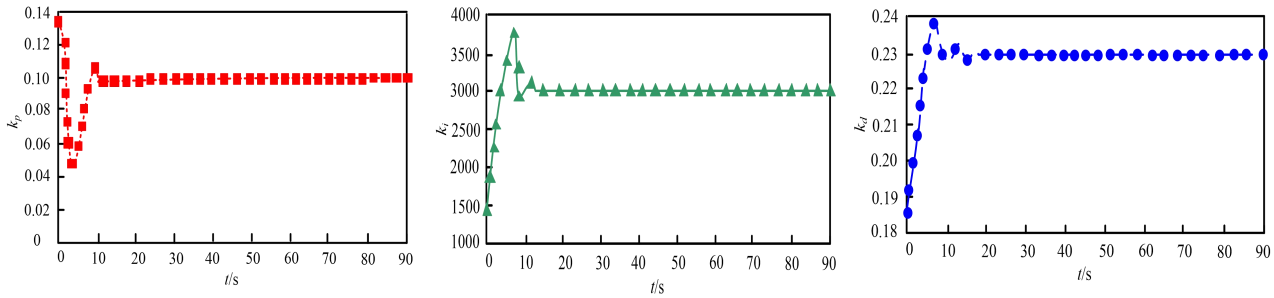


Figure 9. The optimization process of the key parameters of the method in this paper.

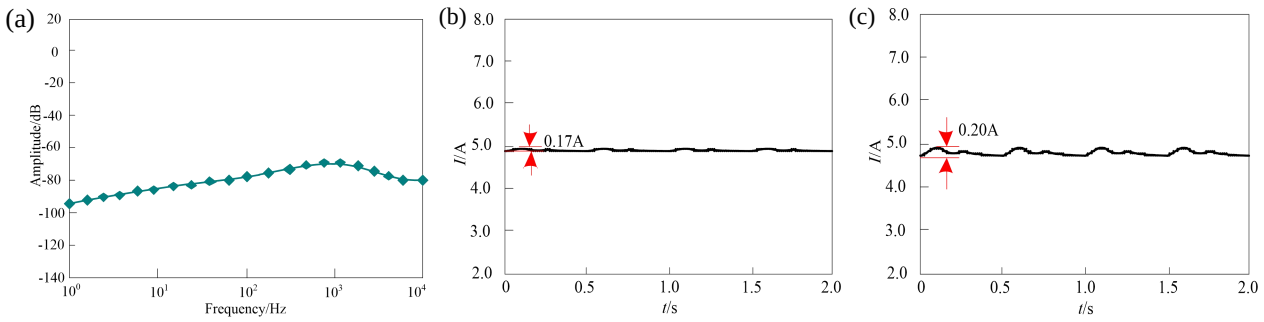


Figure 10. This method controls the output current signal waveform of the experimental charging pile converter. (a) Transfer admittance amplitude; (b) Output current signal waveform of charging pile converter when output voltage is 300V; (c) Output current signal waveform of charging pile converter when output voltage is 500V.

After analyzing Figure 10, it can be learned that the transfer conductor amplitude of the experimental charging pile converter changes significantly compared with that of the previous method, and the amplitude gain of the transfer conductor decreases significantly. The fluctuation degree of the output current signal waveforms of the experimental charging pile converter under different output voltages decreases significantly after the transfer conductor amplitude gain of the converter is controlled as a control quantity, and the signal ripples are more smooth. The maximum ripple fluctuation component of the output current signal is 0.17A and 0.20A respectively, representing reductions of 0.20A and 0.35A respectively compared with that before control, thus indicating that in order to achieve the purpose of smoothing the signal ripple and stabilizing the signal output, the method in this paper can use the transfer-conductance scattering characteristics of the converter as the control parameter to effectively inhibit the ripple components of the output current signal of the experimental rechargeable pile in the presence of low-frequency disturbances.

To verify the effectiveness of this method, a set of comparative experiments is designed for this experiment. The method proposed in reference [7] serves as Control Group 1, while the method proposed in reference [8] serves as Control Group 2, both compared with the method presented in this paper. Steady-state error is chosen as the experimental indicator, and a total of five sets of experiments are conducted, from Experiment Group 1 to Experiment Group 5. The experimental results are shown in Table 3.

Table 3. Comparison of steady-state error experiment table.

| Comparison method | The steady-state error of the experimental group 1 is (%) | The steady-state error of the experimental group 2 is (%) | The steady-state error of the experimental group 3 is (%) | The steady-state error (%) of the experimental group 4 | The steady-state error of the experimental group 5 is (%) |
|---|---|---|---|---|---|
| Control group 1 | 1.2 | 1.5 | 1.8 | 1.7 | 1.6 |
| Control group 2 | 0.9 | 1.1 | 1.3 | 1.5 | 1.8 |
| This paper's method | 0.3 | 0.2 | 0.1 | 0.4 | 0.2 |

From the data comparison in Table 3, it can be seen that the method proposed in this paper demonstrates significant advantages across all experimental groups, with steady-state errors stabilized between 0.1% and 0.4%, none exceeding 0.5%. This is far lower than the 1.2% to 1.8% in Group 1 and 0.9% to 1.8% in Group 2 of the control group. Specifically, in Experiment Group 1, the error of the proposed method is 0.3%, while those for Group 1 and Group 2 are 1.2% and 0.9%, respectively, indicating that the proposed method has a stronger ability to suppress steady-state errors. Therefore, it can be concluded that the control method proposed in this paper can significantly reduce the steady-state error of signals on the output side of the charging pile, and its performance is notably superior to those in literature [7] and [8], providing a reliable solution for high-precision control of charging equipment.

## 4. Conclusion

In practical applications, input signal disturbances in charging piles directly compromise output signal stability. This leads to significant fluctuations in charging current, which can adversely affect the cycle life of connected power battery packs. In order to prevent the emergence of these phenomena, this research concentrates on the

small signal scattering characteristics, utilizing the smooth gradient control method for signal ripples on the output side of charging piles, to conduct the investigation. Through the analysis, we know that the buck converter of the charging pile, as its key module, has a direct influence on the stability of the signal ripple on the output side of the charging pile owing to the small-signal scattering characteristics of the converter, that is, the output side of the converter has a direct influence on the stability of the signal ripple on the output side of the charging pile. Therefore, by constructing a small-signal model of the converter, we analyze the scattering characteristics of the transfer conductor under small-signal perturbation, as well as the correlation between the scattering characteristics and the signal ripple components on the output side of the charging pile. Based on the analytical results, we select the transfer conductor as the control parameter, optimize the parameters of the PID controller by combining with the gradient descent method, and then input the selected control parameter to the optimized PID controller to realize smooth gradient control of the signal ripple on the output side of the charging pile. The practical application results have validated the rationality of the control parameters selected in this study and the effectiveness of the PID controller parameters chosen through the optimized gradient descent method. The maximum ripple fluctuation components of the output current signal under the control of this method are 0.17A and 0.20A respectively representing reductions of 0.20A and 0.35A compared to before control. The steady-state error remains stable between 0.1% and 0.4%, not exceeding 0.5%. Under these conditions, the proposed method can effectively control the ripple component of the current signal on the output side of the experimental charging station, thereby smoothing out the signal ripple on the output side of the charging station. However, in dynamic load changing scenarios, gradient descent with a fixed learning rate may respond slowly and be difficult to adapt to changes in working conditions in real time. Therefore, in order to improve the effectiveness of the proposed method, future research will use intelligent optimization algorithms such as genetic algorithm (GA), particle swarm optimization (PSO), or reinforcement learning (RL) instead of gradient descent to complete the tuning of PID parameters, achieve adaptive online optimization of parameters, and optimize control strategies. In order to better adapt to changes in working conditions, improve control performance, and provide stronger technical support for the popularization of electric vehicles and the development of charging facilities.

## Conflicts of Interest

The authors declare that they have no competing interests

## Data Availability Statement

The raw data can be obtained on request from the corresponding author.


## Funding Declaration

This study did not receive any funding in any form.


## References


[1] Mousaei, Y. Naderi, I.S. Bayram. Advancing State of Charge Management in Electric Vehicles With Machine Learning: A Technological Review. IEEE Access, 2024, 12, 2169-3536. DOI: 10.1109/ACCESS.2024.3378527

[2] Ali, K. Bingi, R. Ibrahim, P.A.M. Devan, M. Omar. Hybrid Fixed and Floating-Point Approach for Implementing PID Controllers on Zynq-7000 FPGA. 2024 IEEE 14th Symposium on Computer Applications & Industrial Electronics (ISCAIE), 2024, 429-434. DOI: 10.1109/ISCAIE61308.2024.10576287

[3] Mousaei. Analyzing locational inequalities in the placement of electric vehicle charging stations using machine learning: A case study in Glasgow. Next Research, 2025, 2(1), 100123. DOI: 10.1016/j.nexres.2024.100123

[4] J. Raji, V. Kamaraj. Investigation of ultra-lift Luo-converter with peak, average and hysteresis current-mode control. Journal of Power Electronics: A Publications of the Korean Institute of Power Electronics, 2021, 21(6), 951-963. DOI: 10.1007/s43236-021-00235-7

[5] S.K. Mohammad, S.N. Soumya, D. Anandarup, Y. Changwoo. Analysis and Control of an Input-Parallel Output-Series Connected Buck-Boost DC–DC Converter for Electric Vehicle Powertrains. IEEE Transactions on Transportation Electrification, 2023, 9(2), 2015-2025. DOI: 10.1109/TTE.2022.3216610

[6] M. Uzam. Optically-isolated analogue output module for a 0-5V to 4-20mA signal converter. Electronics World, 2023, 128(TN.2025), 12-13.

[7] N. Jeelani, A.H. Bhat. Analysis of various modulation techniques for high-frequency isolated single-phase modified quasi-Z-source AC–AC converter-based solid-state transformer. Electrical Engineering, 2024, 106(1), 917-929. DOI: 10.1007/s00202-023-02025-9

[8] S. Lee, W. Hong, T. Kim, G.D. Kim, E.S. Lee, S.H. Lee. Voltage balancing control of a series-resonant DAB converter with a virtual line shaft. Journal of Power Electronics: A Publications of the Korean Institute of Power Electronics, 2022, 22(8),1347-1356. DOI: 10.1007/s43236-022-00466-2

[9] T. Siripan, B. Chanin. Dynamic Modeling and Closed-Loop Control of a Tapped Inductor Buck Converter. Journal of Mobile Multimedia, 2021, 17(4), 673-691. DOI: 10.13052/jmm1550-4646.1749

[10] M. Nahalparvari, M. Asoodar, L. Bessegato, S. Norrga, H.P. Nee. Modeling and Shaping of the DC-Side Admittance of a Modular Multilevel Converter Under Closed-Loop Voltage Control. IEEE Transactions on Power Electronics, 2021, 36(6),7294-7306. DOI: 10.1109/TPEL.2020.3041387

[11] A. Ali, K. Bingi, R. Ibrahim, P.A.M. Devan, K.B. Devika. A review on FPGA implementation of fractional-order systems and PID controllers. AEU-International Journal of Electronics and Communications, 2024, 155-218. DOI: 10.1109/TPEL.2020.3041387

[12] J.D. Hsu, M. Ordonez, W. Eberle, M. Craciun, C. Botting. Enhanced Small-Signal Modeling for Charge-Controlled Resonant Converters. IEEE Transactions on Power Electronics, 2022, 37(2), 1736-1747. DOI:

10.1109/TPEL.2021.3106024
[13] A. Chadha, M.K. Kazimierczuk. Small-Signal Modeling of Open-Loop PWM Tapped-Inductor Buck DC-DC Converter in CCM. IEEE Transactions on Industrial Electronics, 2021, 68(7), 5765-5775. DOI: 10.1109/TIE.2020.2996157
[14] H. Mollaee, S.M. Ghamari, S.A. Saadat, P. Wheeler. A novel adaptive cascade controller design on a buck-boost DC-DC converter with a fractional-order PID voltage controller and a self-tuning regulator adaptive current controller. IET Power Electronics, 2021, 14(11), 1920-1935. DOI: 10.1049/pel2.12159
[15] A.K. Mishra, P.K. Nanda, P.K. Ray, S.R. Das, A.K. Patra. IFGO Optimized Self-adaptive Fuzzy-PID Controlled HSAPF for PQ Enhancement. International Journal of Fuzzy Systems, 2023, 25(2), 468-484. DOI: 10.1007/s40815-022-01382-0
[16] Y. Xue, Y.L. Tong, F. Neri. A hybrid training algorithm based on gradient descent and evolutionary computation. Applied Intelligence: The International Journal of Artificial Intelligence, Neural Networks, and Complex Problem-Solving Technologies, 2023, 53(18), 21465-21482. DOI: 10.1007/s10489-023-04595-4
[17] L. Chizat. Sparse optimization on measures with over-parameterized gradient descent. Mathematical Programming, 2022, 194(1/2), 487-532. DOI: 10.1007/s10107-021-01636-z
[18] H.B. Yuan, Y.B. Kim. Compensated active disturbance rejection control for voltage regulation of a DC-DC boost converter. IET Power Electronics, 2021, 14(2), 432-441. DOI: 10.1049/pel2.12049
[19] P. Rajesh, F.H. Shajin, B.N. Kommula. An efficient integration and control approach to increase the conversion efficiency of high-current low-voltage DC/DC converter. Energy Systems, 2022, 13(4), 939-958. DOI: 10.1007/s12667-021-00452-w
[20] V. Dargahi, A.K. Sadigh, R.R. Khorasani, J. Rodriguez. Active Voltage Balancing Control of a Seven-Level Hybrid Multilevel Converter Topology. IEEE Transactions on Industrial Electronics, 2022, 69(1), 74-89. DOI: 10.1109/TIE.2020.3048288
[21] C. Jiang, A.D. Sinkar, A.M. Gole. Small signal analysis of a grid-forming modular multilevel converter with a novel virtual synchronous generator control. Electric Power Systems Research, 2023, 223, 109621. DOI: 10.1016/j.epsr.2023.109621
[22] M.A. Vaghela, M.A. Mulla. Small-signal model of two-phase interleaved coupled inductor-based high step-up gain converter in DCM. Electrical Engineering, 2023, 105(3), 1565-1583. DOI: 10.1007/s00202-023-01739-0
[23] J. Cui, L.L. Zhang, J. Liu, B. Wang. Fuzzy control Modeling of V2G charging pile with Power quality optimization. Computer Simulation, 2023, 40(3), 116-121+245. DOI: 10.3969/j.issn.1006-9348.2023.03.022
[24] Y.X. Han, M.Z. Ren, Q.L. Ma, C.C. Zhong, J. Chen, X.M. Liang, et al. Research on the Fault Diagnosis Method of Automotive Charging Pile Based on the Improved MLP with SAE. Journal of Electrical Engineering & Technology, 2024, 20(3), 1-13. DOI: 10.1007/s42835-024-02094-1
[25] C. Xu, C. Liu, J.F. Zhang, S.S. Peng. Research on the Development Status and Problems of Third-Party Platform and Operator of Charging Pile. Frontiers in Economics and Management, 2024, 5(7), 51-59. DOI: 10.6981/FEM.202407_5(7).0008